AAPS PharmSciTech (2019) 20: 69
DOI: 10.1208/s12249-018-1279-6

Research Article

An Evaluation of Curcumin-Encapsulated Chitosan Nanoparticles for Transdermal Delivery

Rajesh Sreedharan Nair,[1,3] Andrew Morris,[1] Nashiru Billa,[1] and Chee-Onn Leong[2]

Received 27 September 2018; accepted 10 December 2018; published online 10 January 2019

Abstract. Curcumin-loaded chitosan nanoparticles were synthesised and evaluated *in vitro* for enhanced transdermal delivery. Zetasizer® characterisation of three different formulations of curcumin nanoparticles (Cu-NPs) showed the size ranged from 167.3 ± 3.8 nm to 251.5 ± 5.8 nm, the polydispersity index (PDI) values were between 0.26 and 0.46 and the zeta potential values were positive (+ 18.1 to + 20.2 mV). Scanning electron microscopy (SEM) images supported this size data and confirmed the spherical shape of the nanoparticles. All the formulations showed excellent entrapment efficiency above 80%. FTIR results demonstrate the interaction between chitosan and sodium tripolyphosphate (TPP) and confirm the presence of curcumin in the nanoparticle. Differential scanning calorimetry (DSC) studies of Cu-NPs indicate the presence of curcumin in a disordered crystalline or amorphous state, suggesting the interaction between the drug and the polymer. Drug release studies showed an improved drug release at pH 5.0 than in pH 7.4 and followed a zero order kinetics. The *in vitro* permeation studies through Strat-M® membrane demonstrated an enhanced permeation of Cu-NPs compared to aqueous curcumin solution (p 0.05) having a flux of 0.54 ± 0.03 μg cm^{-2} h^{-1} and 0.44 ± 0.03 μg cm^{-2} h^{-1} corresponding to formulations 5:1 and 3:1, respectively. The cytotoxicity assay on human keratinocyte (HaCat) cells showed enhanced percentage cell viability of Cu-NPs compared to curcumin solution. Cu-NPs developed in this study exhibit superior drug release and enhanced transdermal permeation of curcumin and superior percentage cell viability. Further *ex vivo* and *in vivo* evaluations will be conducted to support these findings.

KEY WORDS: transdermal; curcumin; nanoparticles; *in vitro*; drug release; permeation.

INTRODUCTION

Transdermal drug delivery (TDD) offers many advantages over oral administration such as the avoidance of first-pass metabolism and gastrointestinal disturbances, reduced dosage frequency and more controlled plasma levels (1). However, the major challenge associated with TDD is overcoming the stratum corneum, the outermost layer, which presents a significant barrier. To enhance the permeation through the stratum corneum, it may be necessary to employ various enhancement techniques such as chemical, physical or nano-carriers. Nano-carriers developed for topical or transdermal delivery have a number of advantages over conventional transdermal formulations such as enhanced aesthetics, improved drug stability and prolonged drug release. But although these advantages are evident when formulations are used topically, the use of nano-carriers for transdermal delivery has been limited due to poor skin penetration (2). There has been a belief for many years that intact skin is impenetrable to nanoparticles. However, recent research has demonstrated that nanoparticles can penetrate deep into the skin depending on their size, surface charge and the type of material comprising the nanoparticles (3). Nano-carrier systems such as polymeric nanoparticles and nano-vesicles possess an advantage over other methods in that they promote transdermal permeation without affecting the skin's structure (4). The nanoparticles penetrate the skin through one (or more) of three pathways: transappendageal, *i.e.* hair follicles and sweat glands; intercellular lipid spaces and the transcellular route where drug molecules diffuse through both corneocytes and intercellular lipid lamellae (5).

Curcumin, a natural yellow phenolic compound present particularly in *Curcuma longa* Linn. (turmeric) (6), has demonstrated several pharmacological activities such as anti-inflammatory, antimicrobial, antioxidant, anti-cancer and

[1] School of Pharmacy, University of Nottingham Malaysia, Jalan Broga, 43500, Semenyih, Selangor Darul Ehsan, Malaysia.
[2] Center for Cancer and Stem Cell Research, International Medical University, No.126, Jalan Jalil Perkasa 19, Bukit Jalil, 57000, Kuala Lumpur, Malaysia.
[3] To whom correspondence should be addressed. (e–mail: khyx5rsi@nottingham.edu.my)

antidiabetic effects (6,7). Although curcumin possesses these wide pharmacological activities, a suitable formulation of curcumin is still lacking due to its poor aqueous solubility and instability in alkaline conditions (8). Reports show that, under alkaline conditions, curcumin degrades to trans-6-(4′-hydroxy-3′-methoxyphenyl)-2,4-dioxo-5-hexanal as the major degradation product and ferulic acid, feruloylmethane and vanillin as minor degradation products (9). For these reasons, curcumin exhibits poor absorption after oral administration and undergoes extensive first-pass metabolism (8). Reports reveal that after oral administration of curcumin, 75% is excreted in faeces and traces are found in urine (8). This high degree of chemical instability and low solubility of curcumin hinders its oral administration. Although curcumin has a favourable molecular weight (368 Da) for transdermal delivery, other parameters such as its low aqueous solubility and relatively high log *P* of 3.2 require additional enhancement techniques for skin penetration (10–13). Numerous studies have aimed at improving curcumin bioavailability and stability by a variety of different approaches including formulation into nanoparticles (14), nanogels (15), microemulsions (16,17), nanofibre transdermal patches (18–20), micelles (21,22), polymeric conjugates (23,24) or lipid vesicles (25,26). Polymeric nanoparticles are widely used in drug delivery systems because of their biocompatibility and biodegradability (27). However, the development of curcumin nanoparticles employing natural polymers for transdermal applications has received less attention (28). The solubility and the efficacy of curcumin would be enhanced by formulating into nanoparticles (29). Furthermore, encapsulating curcumin within a polymeric nanoparticle can protect the sensitive drug from environmental factors (3). Chitosan, a natural polysaccharide derived from crustaceans, is widely used in the synthesis of nanoparticles due to its superior biocompatibility and biodegradability. Commercially available chitosan has a degree of deacetylation that ranges from 60 to 100% and the molecular weight ranges from 3800 to 20,000 Da. It is easily degraded *in vivo* and excreted renally (30). Chitosan preparations with a higher degree of deacetylation are preferred in drug delivery systems because a higher degree of deacetylation is synonymous with a greater degradation rate. Chitosan is considered non-toxic and has been certified by the US FDA as safe for use in wound dressings (31). Moreover, at a low pH, it behaves as a cationic polyelectrolyte; therefore, it can easily link with negatively charged cross-linking agents such as sodium tripolyphosphate (TPP). Compared to other methods of nanoparticle synthesis such as emulsion-solvent extraction, spray drying or micelle formation, the ionic gelation technique has some definite advantages. The cross-linking agent TPP is non-toxic and has an excellent gelling capacity. The production method is simple, no toxic chemicals are required and the particle size and zeta potential can be easily modulated by adjusting the concentration of chitosan and TPP (32,33). Furthermore, chitosan nanoparticles (Chi-NPs) have demonstrated permeation enhancement which favour their use as carrier in transdermal drug delivery (34). For successful transdermal delivery, the key factors to consider are the drug solubility in the vehicle, its thermodynamic activity and maximum skin permeation without harming the intact skin. Thus, the approach employed in this study was to develop a novel transdermal formulation of curcumin by combining the benefits of nanoparticulate formulations with the permeation enhancing property of chitosan. This manuscript describes the formulation and the *in vitro* evaluation of curcumin nanoparticles to be ultimately used for transdermal delivery (35).

MATERIALS AND METHODS

Materials

Curcumin (≥ 94% curcuminoid content) and curcumin analytical standard were purchased from Sigma-Aldrich, USA. Acetic acid, sodium acetate, acetonitrile, phosphate-buffered saline (pH 7.4 Tablets) and methanol (HPLC grade) were purchased from Fisher Scientific, UK. Chitosan (low molecular weight) and TPP were purchased from Sigma-Aldrich, USA. The Strat-M® membrane and the MTT [3-(4,5-dimethylthiazol-2-yl)-2,5-diphenyltetrazolium bromide] reagent were purchased from Millipore, Merck, Germany. Dulbecco's modified Eagle's medium (DMEM), Tween 80 and fetal bovine serum were purchased from Nacalai Tesque, Japan. The HaCat cells were from the Center for Cancer and Stem Cell Research, International Medical University, Kuala Lumpur, Malaysia.

Synthesis of Curcumin-Loaded Chitosan-TPP Nanoparticles

Chitosan (0.2% *w*/*v*) solution was prepared in dilute acetic acid (2% *v*/*v*), and the pH was adjusted to 5.0 using 4 M NaOH (36). The solution was stirred (500–1000 rpm on a magnetic stirrer, and an ethanolic solution of curcumin (100 or 500 μg/mL) was added dropwise. Thereafter, varying volumes of the cross-linker (TPP, 0.1% *w*/*v*) solution was added dropwise to this mixture to achieve mass ratios of chitosan and TPP of between 3:1 and 5:1. The suspension obtained was further stirred for 10–45 min at room temperature and then centrifuged at 12857×*g* at 20°C in a centrifuge (Eppendorf 5810 R, Germany) for 20 min to pelletise the nanoparticles. The pellet was subsequently redispersed in deionised water with the cryoprotectant (Trehalose, 5% *w*/*v*), freeze-dried and stored at 2–8°C for further characterisation. The blank nanoparticles were prepared by a similar method without the addition of curcumin.

Particle Size, Zeta Potential and Polydispersity Index (PdI)

The average particle size, zeta potential (ZP) and the PDI of the formulated nanoparticles were measured using a Zetasizer Nano ZS (Malvern Instruments, Malvern, UK). Samples were taken in glass cuvettes and diluted with deionised water (1:3) and analysed at 25°C ($n = 3$). The data obtained were expressed as the mean ± standard deviation.

Flocculation Studies

The blank and the Cu-NPs suspensions were allowed to stand undisturbed at 25°C for 24 h. Samples were withdrawn at 0, 4, 8 and 24 h, and the particle size and ZP were measured for any signs of aggregation or flocculation.

Morphological Characterisation and Energy Dispersive X-Ray Spectroscopy (EdX)

Surface morphology and EDX were determined using field emission scanning electron microscopy (FESEM) (Quanta 400F, FEI, USA) at a voltage of 5 kV coupled with an energy dispersive X-ray detector. A tiny drop of the nanoparticle suspension was placed on double-sided carbon tape and stuck to the imaging stub which was then allowed to dry overnight at ambient temperature. The SEM images and the EDX were recorded for Cu-NPs and Chi-NPs. The EDX of chitosan powder alone was also performed by placing a small quantity directly on the carbon tape.

X-Ray Diffraction (XRD) Analysis

XRD analysis was performed to ascertain the crystallographic structure of the nanoparticle formulation. The diffractograms of curcumin, Chi-NPs and Cu-NPs were obtained using an X'pert Pro X-ray diffractometer (Panalytical, Netherlands) equipped with a radiation source Cu K-alpha operated at 45 kV and 40 mA. The analysis was performed from 5 to 75° with a scanning speed of 0.02°/step and the step time was 0.5 s.

Fourier Transmission Infrared (FTIR) Spectroscopy

The compatibility of curcumin with chitosan and TPP was analysed using FTIR spectrophotometer (Perkin Elmer, USA). Potassium bromide (KBr) was mixed with the sample using a mortar and pestle. The mixture was then compressed using a pellet press at 5 tonnes for 5 min. The KBr pellet was placed in the IR sample holder and the background scan was taken. IR spectra of the samples were recorded over a range of 4000–400 cm^{-1} and peaks were labelled using the Spectrum 5 software (Perkin Elmer) (37). The FTIR spectra were recorded for curcumin, chitosan, TPP, blank and the Cu-NPs.

Differential Scanning Calorimetry (DSC)

DSC thermograms of curcumin, chitosan, TPP, blank and the Cu-NPs were obtained using a DSC Q2000 (TA Instruments, New Castle, USA) equipped with the TA Universal Analysis 2000 software. Approximately 5 to 10 mg of each sample was taken into T zero aluminium pans and sealed with T zero lids and subsequently analysed with a scan rate of 10°C/min from 30 to 350°C. The samples were run with a nitrogen stream of 50 mL/min using an empty reference pan (38,39).

HPLC Method for the Analysis of Curcumin

The method for curcumin analysis was modified from that of Amnon *et al.* (16). The HPLC system (Agilent 1290 series) was equipped with an auto-injector, a quaternary pump and a diode array detector (DAD). The mobile phase consisted of acetonitrile and acetic acid solution (2.0% *v*/*v*) at a ratio of 45:55. Isocratic elution was employed with a flow rate of 1.1 mL/min. Curcumin samples were diluted with methanol, filtered through a 0.45-μm nylon syringe filter (Sartorius, Germany) prior to injection (15 μL**).** A Thermo Fisher Hypersil Gold C18 reverse-phase column (5 μm, 4.6 mm × 250 mm length) was used for all analysis and the column temperature was maintained at 30°C.

Encapsulation Efficiency of the Synthesised Curcumin Nanoparticles (%EE)

Cu-NPs were centrifuged at 12857×*g* at 20°C for 20 min. The supernatant was removed to a separate vial and the sediment containing the nanoparticles was washed twice with methanol to remove any unencapsulated unbound curcumin. The resultant methanol-washed samples and the supernatant were analysed by HPLC to determine the total unbound curcumin. The % EE was calculated as follows: (36,40).

$$\%\mathrm{EE} = \frac{\text{The total amount of curcumin added to the formulation} - \text{Unbound curcumin}}{\text{The total amount of curcumin added to the formulation}} \times 100$$

Swelling Studies

The pH-dependent swelling behaviour of the nanoparticles was studied at pH 5 and pH 7.4 for 24 h. The freeze-dried Chi-NPs and Cu-NPs were dispersed (1 mL) separately in acetate buffer (pH 5) and phosphate-buffered saline (PBS, pH 7.4) in pre-weighed micro-centrifuge tubes. At regular intervals (4, 8 and 24 h), the samples were centrifuged (16,162×*g* at 25°C) for 60 min and the wet mass of the nanoparticles was determined after decanting the supernatant ($n = 3$). The percentage swelling (% Sw) was calculated using the following formula:

$$\%\mathrm{Sw} = \frac{\text{Wet weight} - \text{Initial weight}}{\text{Wet weight}} \times 100$$

Curcumin Release from Nanoparticles

Curcumin release from the nanoparticles was evaluated by using a dialysis bag with molecular weight cut-off of 14,000 Da (Sigma-Aldrich, USA). Curcumin nanoparticles (equivalent to 500 μg curcumin/sample) were dispersed in 3 mL of acetate buffer pH 5.0 or PBS 7.4 containing Tween 80 (0.1% *w*/*v*) and transferred into the dialysis bag. Both ends of the dialysis bag were secured tightly and placed in a glass bottle containing 40 mL of the release medium which was a mixture of 30% ethanol and 70% acetate buffer pH 5.0 or PBS 7.4. The bottle was agitated in a shaker incubator at 180 rpm and 37°C. Samples (1 mL) were withdrawn hourly up to 4 h, followed by every 2 h up to 10 h and finally at 24 h. An equivalent volume of the release medium was replaced after each sampling to maintain a constant volume. Samples were diluted with methanol and the curcumin content was determined by HPLC ($n = 4$). The cumulative percent drug release was plotted against time to obtain the release profile curve.

Drug Release Kinetics

To predict drug release kinetics, the data obtained from the release studies were applied to various kinetic models such as zero order, first order, Higuchi, Korsmeyer-Peppas and the Hixson-Crowell Model.

Zero-Order

Zero-order kinetics describes the constant release of drug from a formulation and is independent of the time or the concentration; zero-order release is represented by the equation: $C_0 - C_t = K_0 t$, where C_0 is the initial drug concentration, C_t is the amount of drug released at time 't' and K_0 is the zero order rate constant. The data fitting to this model was assessed by plotting the cumulative percentage of drug release against time.

First-Order

Here, the rate of release is dependent on the initial drug concentration and time. The release of drug from the formulation follows an exponential manner as described by the equation: $\text{Log } C = \text{Log } C_0 - K_t/2.303$ where C_0 is the initial drug concentration, t is time and K_t is the first-order rate constant. The data obtained were plotted as cumulative log percentage of drug remaining *versus* time.

Korsmeyer-Peppas

The Korsmeyer-Peppas model predicts the drug release mechanism from polymeric systems. The data were plotted as the log of cumulative drug release (%) against the log of time represented by the following equation:

$$\frac{C_t}{C_\infty} = Kt^n$$

where $C_t/C\infty$ is the fraction of drug release at time t and K is rate constant.

Higuchi Model

This model often describes drug release from matrix systems. Data obtained were fitted into this model by plotting the cumulative percentage of drug release *versus* square root of time: $C_t = K_H \sqrt{t}$, where C_t is drug released at time t and K_H is the Higuchi rate constant.

Hixson-Crowell Model

This model describes drug release which is dependent on the surface area and volume of the particles and is represented by the following equation:

$$C_0^{1/3} - C_t^{1/3} = K_H Ct$$

K_H is the rate constant, C_0 is the initial drug concentration and C_t is the drug release at time t. Data obtained from the release study were fitted into this model by plotting the cube root of the percentage drug remaining *versus* time.

In vitro Permeation Studies of Cu-NPs Using Strat-M Membrane

The *in vitro* permeation of Cu-NPs was performed using Strat-M® membrane. Static Franz-type diffusion cells (Permegear, USA), having donor and receptor capacities of approximately 1 and 2 mL, respectively, with an effective diffusion area of approximately 0.95 cm^2, were used for the permeation experiments. After applying silicone grease as a sealant over the flanges of the donor and receptor compartments, the membrane was fixed securely in between the donor and the receptor compartment and fastened with a horseshoe clamp. The receptor compartment contained phosphate-buffered saline 7.4 (PBS) with 1% Tween 80 and was stirred with a miniature magnetic stirring rod to help maintain sink conditions (41). The diffusion cells were placed on a submersible magnetic stirrer block and immersed in a water bath maintained at 37°C. Cu-NPs (equivalent to 500 μg of curcumin) were dispersed in acetate buffer pH 5 and placed in the donor compartments. Two hundred-microliter samples were withdrawn from the receptor compartments, at predetermined time points up to 72 h. An equal volume of fresh receptor medium was replaced immediately to each cell to maintain the receptor volume. Samples were stored in a refrigerator at 4–8°C prior to HPLC analysis. Permeation profile curves were generated by plotting the cumulative amount permeated (μg/cm^2) against time (h). The steady-state flux (J) which represents the amount of curcumin permeated per unit area was determined from the gradient of the linear portion of the plot (42,43).

Cytotoxicity Assay

The HaCat cells were maintained in Dulbecco's modified Eagle's medium (DMEM) (Nacalai Tesque, Japan) media with 10% fetal bovine serum (Nacalai Tesque, Japan) and 1% penicillin-streptomycin (Nacalai Tesque, Japan) at 37°C in an incubator with 5% CO_2. The cytotoxicity of the various nanoparticle formulations was determined using the MTT [3-(4,5-dimethylthiazol-2-yl)-2,5-diphenyltetrazolium bromide] assay. The HaCat cells were seeded in a 96-well plate (5×10^3 cells/well) and incubated for about 24 h, thereby allowing the cells to adhere to the plates. The culture medium was subsequently removed and the cells were treated with the drug solutions or Cu-NPs after diluting with DMEM media. Untreated cells were used as a control and maintained under the same experimental conditions. After 24 h of incubation, 20-μL MTT (5 mg/mL in sterile PBS 7.4) solution was added to each well and incubated for a further 4 h at 37°C. The MTT reagent reacts with the mitochondria of the viable cells and a purple coloured formazan is formed. The media was removed from each well and 100 μL of DMSO was added to dissolve the formazan crystals and the absorbance was measured at 570 nm using a microplate reader (Biotek Instruments, Inc. USA.) ($n = 4$). The percentage cell viability was calculated as follows:

Cell viability (%) = (absorbance of the treated cell/absorbance of the control) × 100.

Statistical Analyses

Statistical analysis was done using the Graph-Pad Prism 7 software. All values are expressed as a mean ± standard deviation. The statistical significance between the sets of data was tested by one-way analysis of variance (ANOVA)

followed by post hoc Tukey-HSD (honestly significant difference) with $p < 0.05$ considered significant.

RESULTS AND DISCUSSION

Synthesis and Optimisation of the Curcumin Nanoparticles

The Cu-NPs were successfully synthesised by the ionic gelation method using biodegradable polymer chitosan and TPP as the cross-linking agent. TPP is less toxic than other cross-linkers such as glutaraldehyde which can cause antigenicity (44). Varying mass ratios of chitosan and TPP were employed to achieve uniform particle size with a low PDI and high positive zeta potential. The polyanions ($P_3O_{10}^{5-}$) help establish the inter- and intramolecular linkages with the amino group (NH_2^+) of chitosan, and this forms the basis of the ionic gelation technique. In this study, chitosan and TPP concentrations were optimised as 0.2% *w/v* and 0.1% *w/v*, respectively, where the pH of chitosan solution was maintained at 5.0 (45). Wen Fan *et al.* report the influence of solution pH on particle size distribution. As the pH of the chitosan solution fell below 4.5, a heterogeneous size distribution was observed. Conversely, when the pH exceeded 5.5 microparticles were produced (46). The relationship between the solution pH and degree of protonation of chitosan can be explained by the Henderson-Hasselbalch equation (47); as the pH of the solution rises from 4.7 to 8.0, the degree of protonation was found to decrease from 100 to 0% (46). The pK_a value of the amino group in chitosan ranges from 6.2 to 6.5 and above this point deprotonated amino groups start to predominate and the ability to crosslink with tripolyphosphoric ions is suppressed. The concentration of acetic acid used in the chitosan solution plays an important role in determining the homogeneity of the dispersion. In this study, 2% *v/v* acetic acid solution was used throughout because the acetic acid concentration should be kept at least twice the concentration of chitosan to achieve monodispersed nanoparticles (35).

The particle size of the blank nanoparticles ranged from 161.5 ± 3.8 to 166.5 ± 1.9 nm whereas the size of Cu-NPs ranged from 167.3 ± 1.9 (3:1) to 251.5 ± 5.8 nm (5:1). The particle size increased with the increase in chitosan-TPP mass ratio which is in agreement with other reports (32). The higher TPP concentration used in the formulation (3:1) might help attract chitosan molecules for stronger intramolecular interactions that resulted in the formation of smaller particles. Similarly, the particle size increased proportionately with the increase in drug loading (100 to 500 μg) and Cu-NPs were significantly larger than the blank nanoparticles (p 0.05) as depicted in Fig. 1a. Figure 2a demonstrates the effect of stirring speed (rpm) on the mean nanoparticle size. There were no significant changes observed in the particle size when the stirring speed was increased from 400 to 700 rpm. However, a significant difference (p 0.05) was seen when the stirring speed was increased to 1000 rpm. Reports suggest that high shearing forces may lessen the repulsive forces between the particles and facilitate aggregation (45). The effect of stirring time on particle size was also evaluated and the results showed no significant differences whether stirred for 10, 20 or 45 min (Fig. 2b). This indicates that the nanoparticles were formed upon the addition of TPP even with shorter stirring time. It is desirable to keep the PDI values of the dispersion as low as possible to achieve monodispersity; PDI values > 0.5 generally show broader size distribution. It was therefore desirable to maintain the PDI as low as possible and the observed value was 0.46 for all formulations. From the size analysis results, it is evident that the average particle size of all the formulations was below 300 nm which is ideal for the transdermal delivery (35,45).

The ZP values of blank nanoparticles ranged between + 17.9 and + 21.3 mV whereas the values for curcumin-loaded nanoparticles ranged between + 18.1 and + 20.23 mV (Fig. 1b). No significant differences were observed between the zeta potential of the blank and the curcumin-loaded nanoparticles. This was perhaps because the concentration of chitosan was kept constant for all formulations. The positive zeta potential is attributed due to the presence of the amino group of chitosan. The high positive charge is necessary to prevent aggregation and helps the nanoparticle to interact with the negative charges of the skin. Taveira *et al.* reported an enhanced permeation of doxorubicin from chitosan gel when used for iontophoresis, suggesting the interaction of chitosan with the negatively charged groups present in the skin (34). Studies also report the mucoadhesive and absorption enhancing properties of chitosan and its derivatives through intestinal epithelial cells (48). These compounds may loosen the tight junctions of intestinal epithelial cells and easily cross the epithelial membrane (49). Although the structure and composition of epithelial cells of the stratum corneum may differ from the intestinal epithelial cells, they share some common features that both possess tight intercellular junctions (50,51). Flocculation studies of the blank and the Cu-NPs were conducted over 24 h. Two formulations (3:1 and 5:1) of blank and drug-loaded nanoparticles were selected for this study. The statistical analysis showed no significant changes in the particle size, ZP or PDI, thus indicating the short-term stability of the formulation.

FESEM and EDX

The FESEM images of the optimised Cu-NPs displayed a spherical shape with a smooth surface (Fig. 3a). The particles appeared sufficiently separated, therefore reducing the chance of aggregation and therefore ensuring adequate stability. The particle diameter revealed in the SEM image was in agreement with the data obtained from the Zetasizer as reported in the previous section.

The EDX analysis confirmed the presence of phosphorus in the nanoparticles, suggesting the presence of TPP in the nanoparticles. The chitosan powder had shown a composition of carbon (C; 53.9%), nitrogen (N; 7.5%) and oxygen (O; 38.6%). Additionally, the Chi-NPs and Cu-NPs were shown to contain phosphorus (P) and sodium (Na), which was attributed to the TPP. The observed elemental composition in Chi-NPs (32.9% C, 48.4% O, Na 9.9%, 5.2% N and 3.6% P) and Cu-NPs (36.2% C, 47.8% O, Na 8.0%, 5.1% N and 2.9% P) followed a similar fashion (Fig. 3b). The percentage composition of phosphorus detected in the nanoparticles was similar to other reports by Pinho *et al.* (52) (2.2% P) and Grenha *et al.* (53) (2.9% P).

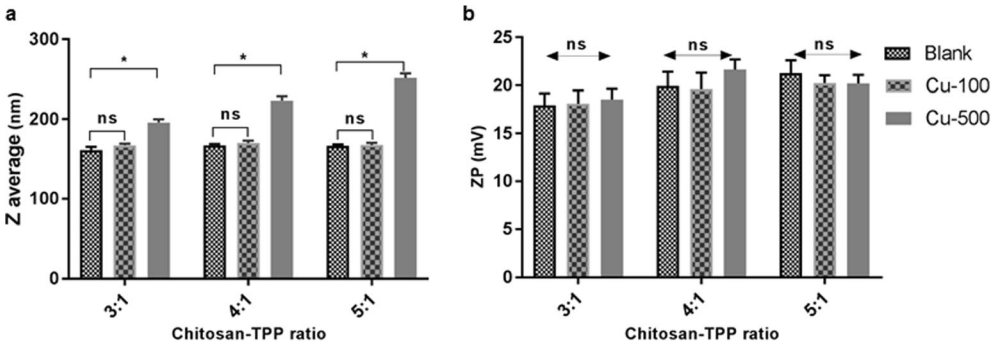

Fig. 1. Z- average (**a**) and zeta potential (**b**) of three different formulations of blank and Cu-NPs containing 100 and 500 μg of curcumin. Mean ± SD, $n = 3$ (*ns* not significant; $*p < 0.033$)

XRD Analysis

The XRD diffractogram of curcumin shows multiple peaks between 5 and 30° which were mainly attributed to its crystalline nature. These characteristic peaks had disappeared in the Cu-NPs (Fig. 4), suggesting the transformation of the crystalline nature of curcumin to an amorphous state (54). This change in physical characteristics may perhaps result from the molecular interactions between curcumin and chitosan occurring during formulation. A similar XRD pattern of curcumin-PLGA nanoparticles was reported by Chereddy *et al.* (55). It is worthwhile to note that the physical transformation of curcumin in the Cu-NPs did not affect the structural characteristics of curcumin, as confirmed by the FTIR analysis.

FTIR Analysis

Figure 5 shows the FTIR spectra of curcumin, chitosan, TPP, a physical mixture of curcumin-chitosan-TPP and the Cu-NPs. The principal peaks of curcumin were observed at 3504.2 and 2943.9 cm^{-1} which correspond to the -OH stretch and vibration of C-H bonds, respectively. An aromatic (C=C) stretching of curcumin was observed between 1400 and 1600 cm^{-1}. A distinguishing peak of chitosan was observed at 3448.0 cm^{-1} which is mainly due to the –NH stretching vibration. Furthermore, weaker bands were observed at 2880.6 and 1651.8 cm^{-1} corresponding to –CH stretching and $–NH_2$, groups respectively (56). The spectrum of TPP demonstrated characteristic peaks at 1211.4 and 1158.5 cm^{-1} which correspond to phosphate stretching (P-O-C) and vibration (P=O) (57). The principal peaks of curcumin and other additives used in the formulation appeared exactly in the same position in the physical mixture and the nanoparticles. Nevertheless, the peaks seem to be smoother and show a slight shift in the Cu-NPs, indicating chemical shifts arising from the ionic interaction between the drug, polymer and the cross-linker. Significant band broadening was observed in the region 3600 to 3400 cm^{-1}, attributed to intermolecular hydrogen bonding (58). In general, the FTIR results confirm the interaction between the drug and other additives and corroborate the presence of curcumin in the nanoparticle formulation.

DSC Analysis

DSC thermograms of curcumin, chitosan, TPP and curcumin-loaded chitosan nanoparticles are shown in Fig. 6. The thermogram of curcumin shows a sharp endothermic peak at 178.5°C which corresponds to the melting point of curcumin. Chitosan shows both endothermic and exothermic peaks. An endothermic peak at 100°C is probably due to water loss from the hydrophilic groups; whilst an exothermic peak at 306.0°C indicates degradation due to dehydration and depolymerization (59,60). Furthermore, a weak endothermic peak in the Cu-NPs at 225°C may result from the endothermic shift of curcumin; this suggests that curcumin was successfully retained in the nanoparticle formulation (61). TPP shows a weak endothermic peak at 118.6°C corresponding to the melting point and this peak was not present in the Cu-NP thermograms, probably due to the ionic interaction with chitosan. Shifts of exothermic and endothermic peaks

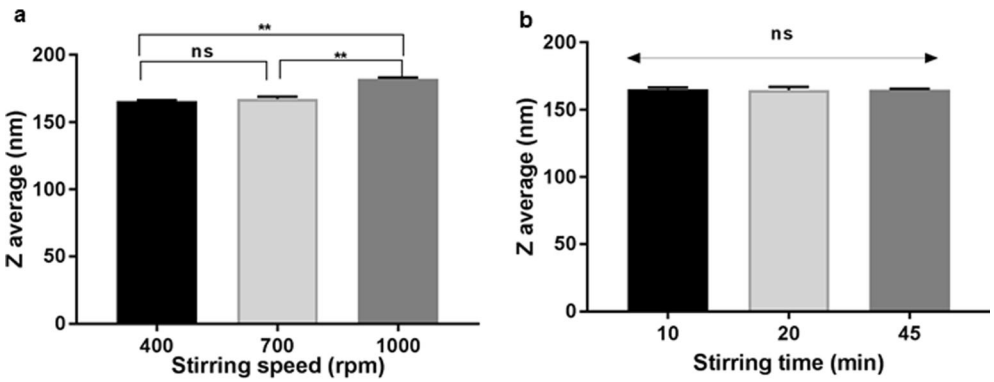

Fig. 2. Effect of stirring speed (**a**), and the effect of stirring time (**b**) on the particle size of Chi-NPs (3:1). Mean ± SD, $n = 3$ (*ns* not significant; $**p < 0.002$)

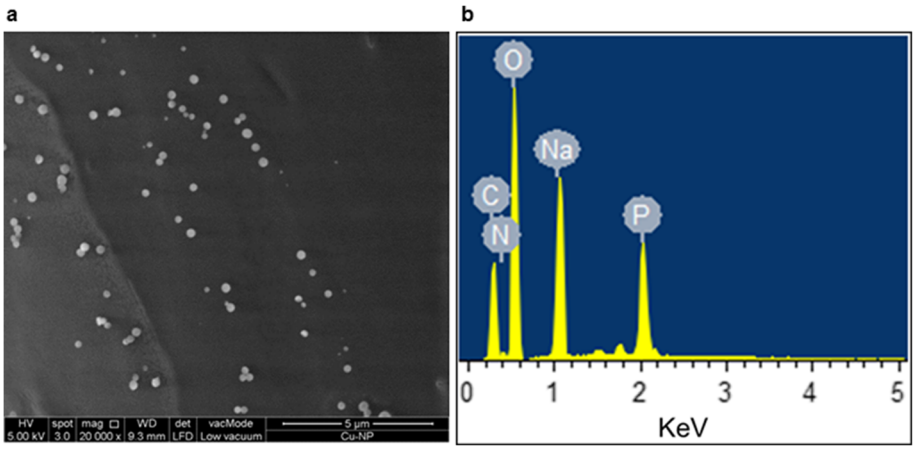

Fig. 3. FSEM image of Cu-NPs (**a**) and EDX analysis (**b**) showing the elements present in Cu-NPs

are usually associated with interactions between drug and polymers (59). The DSC and XRD analyses suggest that the encapsulated curcumin in the nanoparticles would have changed from its original crystalline nature to an amorphous state, confirming the interaction between the drug and the polymer and hence successful encapsulation (14).

Encapsulation Efficiency of the Curcumin Nanoparticles

The encapsulation efficiency of the formulations was determined as 80.4, 80.2 and 88.4% corresponding to the formulations 5:1, 4:1 and 3:1, respectively. Studies have shown that encapsulation efficiency may vary according to the concentration of chitosan and TPP used (62). In this work, we have maintained the chitosan concentration constant and the amount of TPP was varied among the formulations. The formulation 3:1 had shown the highest encapsulation (88.4%). This may be due to the higher TPP content in this formulation, which may have helped interact with a large number of chitosan molecules permitting more curcumin in the nanoparticle core.

Swelling Studies

The swelling behaviour of blank nanoparticles and Cu-NPs was determined at pH 5.0 and pH 7.4. The nanoparticles showed increased swelling in the more acidic pH 5.0 than at pH 7.4. The swelling index of the blank nanoparticles was determined as 78.9 ± 0.7% and 68.8 ± 0.6% at pH 5.0 and pH 7.4, respectively. Similarly, the Cu-NPs had shown a swelling index of 70.4 ± 0.6% (pH 5.0) and 62.4 ± 1.0% (pH 7.4). The enhanced swelling of nanoparticles at pH 5.0 is mainly due to the superior swelling behaviour of chitosan at acidic pH, particularly below its p*K*a 6.2. At this pH, the highly protonated amino groups repel each other creating voids, thereby permitting the entry of water molecule into the

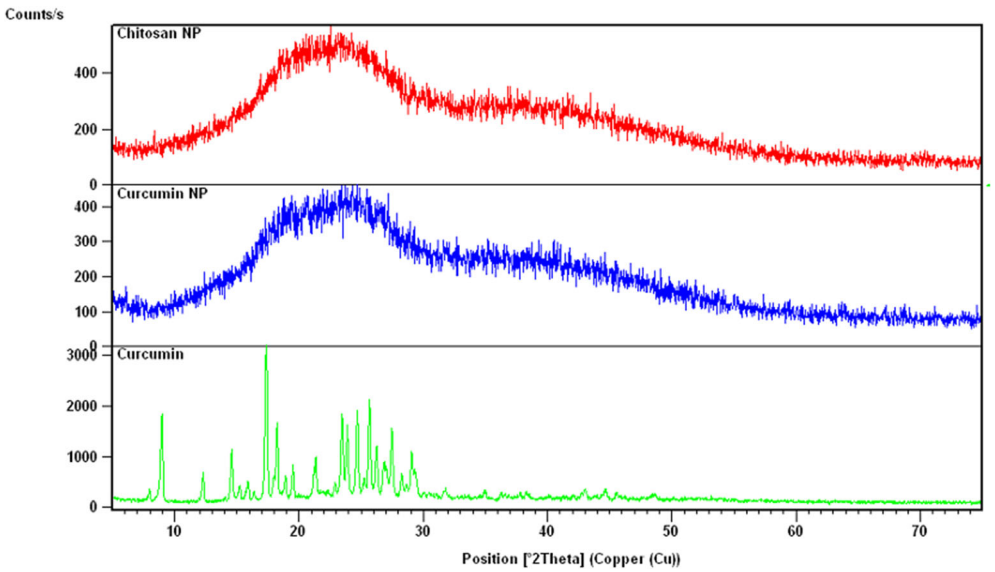

Fig. 4. XRD patterns of curcumin, Chi-NPs and Cu-NPs

Fig. 5. FTIR spectra of curcumin, chitosan, TPP, curcumin-chitosan-TPP physical mixture and Cu-NPs

nanoparticle core and swells. On the contrary, at higher pH, chitosan molecules shrink due to low protonation (63). The blank nanoparticles show greater swelling index than the Cu-NPs at both pH conditions; the drug conjugation and the reduced number of free functional groups in Cu-NPs may be attributed to this.

Drug Release Study of Curcumin Nanoparticles

Drug release from nanoparticles usually takes place *via* one or more mechanisms such as surface erosion, diffusion, disintegration or desorption (64). Drug release studies from the Cu-NPs were performed at pH 5.0 and pH 7.4, simulating the skin pH and physiological pH, respectively. It is evident from the release curve (Fig. 7) that no initial burst release was seen at either pH; instead, a controlled release was observed over time, suggesting the homogeneous encapsulation of curcumin in the nanoparticles. The initial burst release of drug from nanoparticles usually occurs due to drug deposition on the surface of nanoparticles as a result of poor encapsulation (64). Samples were withdrawn initially every hour up to 4 h with the aim of determining whether there was an initial rapid release from the formulations. At pH 5, 41.5 ± 1.1% of

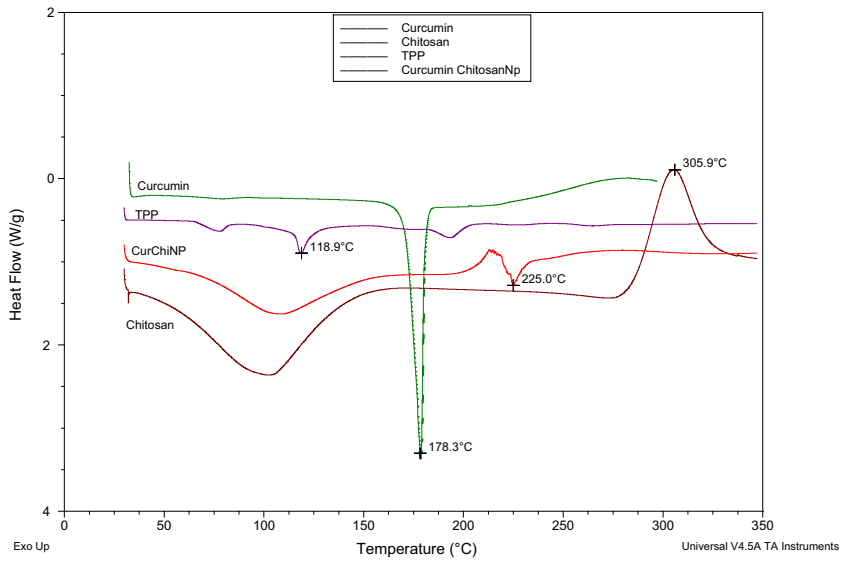

Fig. 6. Dsc thermogram of curcumin, TPP, chitosan and Cu-NPs

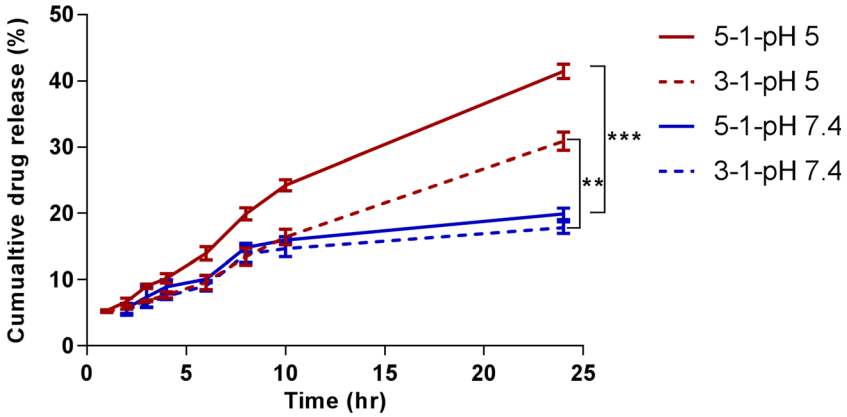

Fig. 7. Curcumin release from Cu-NPs (3:1 and 5:1) at pH 5 and pH 7.4, showing enhanced drug release at pH 5. Mean ± SD, $n = 4$

curcumin was released by 24 h, whereas only about 19% drug release occurred at pH 7.4 over the same period. Between the two formulations, the ratio 5:1 showed a slightly enhanced drug release which was possibly due to the greater swelling capacity of larger nanoparticles and the low TPP content. The cross-linking agent plays a major role in drug release; Ko *et al.* reported that an increase in TPP concentration had decreased felodipine release from chitosan-TPP microparticles (65). The difference in drug release observed at two different pH conditions (pH 5.0 and pH 7.4 may be attributed to the pH-dependent swelling behaviour of chitosan (62). The swelling of chitosan allows the release medium to penetrate inside the polymer matrix and act as a plasticiser converting the glassy polymer to a more rubbery form and subsequently leading to improved drug release from the nanoparticle structure (66). The high curcumin release observed at pH 5 may also be attributed to its enhanced stability in the acidic environment as compared to neutral or alkaline conditions (9). The drug release mechanism was investigated by fitting the release data into various kinetic models; the regression coefficient (R^2) values of the different models are depicted in Table I. The R^2 value close to 1 gives an indication of best fit to that model. The release data obtained at pH 5.0 most closely fits zero order kinetics with R^2 values of 0.9755 and 0.9891 corresponding to the formulations 3:1 and 5:1, respectively. Conversely, the release data at pH 7.4 showed the best fit to Higuchi's model indicating the diffusion mechanism. The zero order release of curcumin observed at pH 5.0 is suitable for the transdermal delivery of these formulations. As the skin pH ranges between 4.8 and 6.0, an enhanced release of curcumin from the nanoparticles at pH 5 may enhance skin permeation of the drug.

Table I. The R^2 Value of Various Drug Release Kinetic Models of Two Different Formulations (3:1 and 5:1) at pH 5 and pH 7.4

Kinetic model	5:1		3:1	
	pH 5	pH 7.4	pH 5	pH 7.4
Zero order	0.9891	0.9165	0.9755	0.9115
First order	0.9802	0.9264	0.971	0.8696
Higuchi	0.9434	0.9510	0.9148	0.9566
Korsmeyer-Peppas	0.9485	0.8765	0.9025	0.8698
Hixson-Crowell	0.9826	0.9295	0.9563	0.931

In vitro Permeation Using Strat-M® Membrane

The *in vitro* permeation studies give significant insight into the behaviour of formulations *in vivo*. *In vitro* permeation of the formulations (3:1 and 5:1) was performed using Strat-M® membrane. Strat-M is made of polyester sulfone arranged as multiple layers mimicking the skin structure including a tough outer layer. Takashi *et al.* evaluated the permeation of 13 chemical compounds having a wide range of molecular weights and lipophilicities using Strat-M®, excised human skin or hairless rat skin (67). The permeation of these compounds through Strat-M® was comparable with the results obtained using excised human skin or rat skin, and suggests that Strat-M® could be an alternative to excised human or rat skin in conducting permeation studies using nanocarriers. Thermodynamic activity in the donor phase influences the diffusion rate of drug molecules across a membrane. Maintaining a saturated drug concentration in the donor phase ensures a maximal thermodynamic activity and greatest flux. A steady linear increase in the cumulative drug permeation throughout the course of the experiment indicates that drug depletion is unlikely to have had a significant effect on the permeation rate. Isotonic phosphate-buffered saline (pH 7.4) is a generally accepted receptor fluid for *in vitro* experiments employing artificial skin membranes or non-viable skin. However, *in vitro* experiments are challenging when dealing with very hydrophobic drugs like curcumin. Therefore, in order to ensure that sink conditions are maintained in the receptor compartment, the addition of a solubilising agent or co-solvent is often employed (68). However, it is important that such additives cause no damage to the integrity of the membrane that is being used. Studies report that co-solvents such as ethanol can disturb the skin integrity (69) and a previous report reveals that 50% ethanol in the receptor medium enhances the permeation of both hydrophilic and lipophilic compounds across rat skin. Therefore, the use of surfactants can be preferable to a co-solvent because of their ability to solubilise a variety of drugs with less effect on membrane integrity whilst also permitting drug content analysis without complex procedures. The addition of 1% Tween 80 to the receptor medium has been demonstrated to enhance

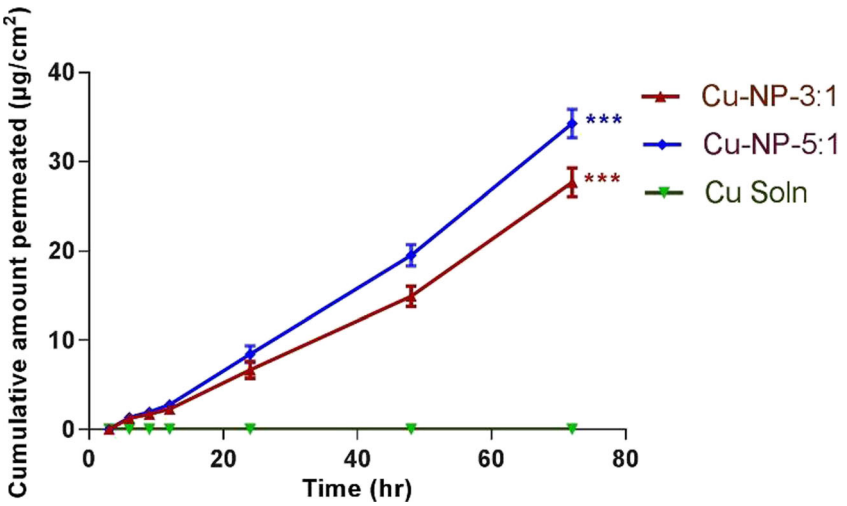

Fig. 8. Permeation of Cu-NPs (3:1 and 5:1) through Strat-M membrane, showing superior permeation compared to the control curcumin solution. Mean ± SD, $n = 4$ (*ns* not significant; ***$p < 0.001$)

curcumin solubility and help maintain sink conditions (70). Curcumin degrades rapidly in neutral to alkaline pH; however, previous studies suggest that polysorbates such as Tween 80 significantly enhance the stability of curcumin through micelle formation (71,72). Figure 8 demonstrates an enhanced permeation of Cu-NPs. The permeation of curcumin from both the formulations (3:1 and 5:1) was significantly higher than the control (curcumin solution) (p 0.05). The poor solubility of curcumin in the donor phase might be the limiting factor for the control solution. The cumulative amount of curcumin permeated at 72 h was 34.3 ± 1.6 µg cm^{-2} and 27.7 ± 1.7 µg cm^{-2} for the formulations 5:1 and 3:1, respectively. The flux values were calculated as 0.54 ± 0.03 µg cm^{-2} h^{-1} (5:1) and 0.44 ± 0.03 µg cm^{-2} h^{-1} (3:1). Studies report the permeation of curcumin nanoparticles using the porcine skin and the reported flux was 0.61 µg cm^{-2} h^{-1}, which is comparable with our results (15). The nanosize of the formulation and the chitosan content may be contributing factors in the enhanced permeation of curcumin. Furthermore, chitosan has the potential to retain water and this may impact upon the structure of the stratum corneum. Reports reveal the enhanced permeation of acyclovir through the porcine skin when the chitosan content in the formulation is increased (73).

Cytotoxicity Assay

The cytotoxicity of the nanoparticles, curcumin solution and the blank nanoparticles were performed on HaCat cells using MTT assay. At a lower concentration (2.5 µg/mL), there were no significant differences in the cell viability between the blank, curcumin solution and the Cu-NPs. However, significant differences were observed at higher concentrations compared to the blank formulation (Fig. 9). The percentage cell viability with Cu-NPs (10 µg/mL) was significantly higher than curcumin solution ($p < 0.002$), whereas the blank chitosan nanoparticles did not show any significant cytotoxicity. Studies show that curcumin induces apoptosis on HaCat cells (74). However, the effect could be reduced in the presence of

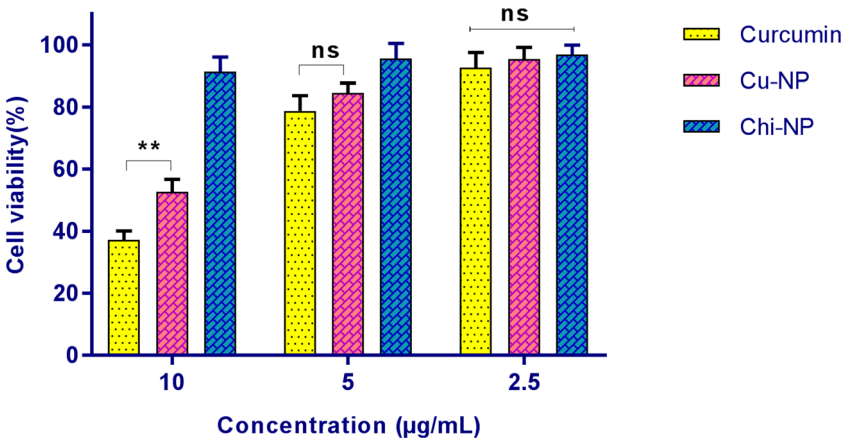

Fig. 9. Percentage cell viability of HaCat cells on treatment with curcumin solution, Chi-NPs and Cu-NPs at three different concentrations (2.5 µg/mL, 5 µg/mL, 10 µg/mL), shows enhanced cell viability of Cu-NPs than curcumin solution. Mean ± SD, $n = 4$ (*ns* not significant; **$p < 0.002$)

antioxidants (75). Chitosan and its derivatives have shown to possess antioxidant activities and this may be attributed to the enhanced cell viability reported with Cu-NPs. The MTT assay results support the safety of the formulation against HaCat cells and suggest the suitability of Cu-NPs for transdermal applications.

CONCLUSION

Curcumin-loaded chitosan nanoparticles were successfully synthesised and evaluated *in vitro*. The EDX and FTIR analyses confirmed the successful formation of the nanoparticles. The zero-order drug release observed at pH 5.0 support the appropriateness of this formulation for transdermal delivery. The cytotoxicity studies showed enhanced cell viability of Cu-NPs compared to curcumin solution. To conclude, the formulated Cu-NPs have shown superior permeation through the Strat-M membrane *in vitro* compared to the control. However, further *ex vivo* and *in vivo* evaluations will be required to support these findings.

ACKNOWLEDGEMENTS

The authors would like to acknowledge the Faculty of Science at the University of Nottingham Malaysia (UNM) for the financial support of this project.

COMPLIANCE WITH ETHICAL STANDARDS

Conflict of Interest The authors declare that they have no conflict of interest.

Publisher's Note Springer Nature remains neutral with regard to jurisdictional claims in published maps and institutional affiliations.

REFERENCES

1. Ren C, Fang L, Ling L, Wang Q, Liu S, Zhao L, *et al.* Design and in vivo evaluation of an indapamide transdermal patch. Int J Pharm. 2009;370:129–35.
2. Zhao Y, Brown MB, Jones SA. Pharmaceutical foams: are they the answer to the dilemma of topical nanoparticles? Nanomedicine. 2010;6:227–36. https://doi.org/10.1016/j.nano.2009.08.002.
3. Palmer BC, DeLouise LA. Nanoparticle-enabled transdermal drug delivery systems for enhanced dose control and tissue targeting. Molecules. 2016;21:1719.
4. Williams AC, Barry BW. Penetration enhancers. Adv Drug Deliv Rev. 2004;56:603–18. https://doi.org/10.1016/j.addr.2003.10.025.
5. Pegoraro C, MacNeil S, Battaglia G. Transdermal drug delivery: from micro to nano. Nanoscale. 2012;4:1881–94.
6. Naksuriya O, Okonogi S, Schiffelers RM, Hennink WE. Curcumin nanoformulations: a review of pharmaceutical properties and preclinical studies and clinical data related to cancer treatment. Biomaterials. 2014;35:3365–83.
7. Sun M, Su X, Ding B, He X, Liu X, Yu A, *et al.* Advances in nanotechnology-based delivery systems for curcumin. Nanomedicine. 2012;7:1085–100.
8. Wang Y-J, Pan M-H, Cheng A-L, Lin L-I, Ho Y-S, Hsieh C-Y, *et al.* Stability of curcumin in buffer solutions and characterization of its degradation products. J Pharm Biomed Anal. 1997;15:1867–76. https://doi.org/10.1016/S0731-7085(96)02024-9.
9. Sharma RA, Gescher AJ, Steward WP. Curcumin: the story so far. Eur J Cancer. 2005;41:1955–68. https://doi.org/10.1016/j.ejca.2005.05.009.
10. Chaudhary H, Kohli K, Kumar V. Nano-transfersomes as a novel carrier for transdermal delivery. Int J Pharm. 2013;454:367–80.
11. Jose A, Labala S, Ninave KM, Gade SK, Venuganti VVK. Effective skin cancer treatment by topical co-delivery of curcumin and STAT3 siRNA using cationic liposomes. AAPS PharmSciTech. 2018;19(1):166–75. https://doi.org/10.1208/s12249-017-0833-y.
12. Alves TF, Chaud MV, Grotto D, Jozala AF, Pandit R, Rai M, *et al.* Association of silver nanoparticles and curcumin solid dispersion: antimicrobial and antioxidant properties. AAPS PharmSciTech. 2018;19:225–31. https://doi.org/10.1208/s12249-017-0832-z.
13. Raju YP, N H, Chowdary VH, Nair RS, Basha DJ, N T. In vitro assessment of non-irritant microemulsified voriconazole hydrogel system. Artif Cells Nanomed Biotechnol. 2017;45:1539–47. https://doi.org/10.1080/21691401.2016.1260579.
14. Rachmawati H, Yulia LY, Rahma A, Nobuyuki M. Curcumin-loaded PLA nanoparticles: formulation and physical evaluation. Sci Pharm. 2016;84(1):191–202.
15. Mangalathillam S, Rejinold NS, Nair A, Lakshmanan V-K, Nair SV, Jayakumar R. Curcumin loaded chitin nanogels for skin cancer treatment via the transdermal route. Nanoscale. 2012;4:239–50.
16. Sintov AC. Transdermal delivery of curcumin via microemulsion. Int J Pharm. 2015;481(1–2):97–103. https://doi.org/10.1016/j.ijpharm.2015.02.005.
17. Liu CH, Chang FY, Hung DK. Terpene microemulsions for transdermal curcumin delivery: effects of terpenes and cosurfactants. Colloids Surf B. 2011;82:63–70. https://doi.org/10.1016/j.colsurfb.2010.08.018.
18. Ariamoghaddam AR, Ebrahimi-Hosseinzadeh B, Hatamian-Zarmi A, Sahraeian R. In vivo anti-obesity efficacy of curcumin loaded nanofibers transdermal patches in high-fat diet induced obese rats. Mater Sci Eng C. 2018;92:161–71. https://doi.org/10.1016/j.msec.2018.06.030.
19. Ravikumar R, Ganesh M, Senthil V, Ramesh YV, Jakki SL, Choi EY. Tetrahydro curcumin loaded PCL-PEG electrospun transdermal nanofiber patch: preparation, characterization, and in vitro diffusion evaluations. J Drug Deliv Sci Technol. 2018;44:342–8. https://doi.org/10.1016/j.jddst.2018.01.016.
20. Ravikumar R, Ganesh M, Ubaidulla U, Young Choi E, Tae Jang H. Preparation, characterization, and in vitro diffusion study of nonwoven electrospun nanofiber of curcumin-loaded cellulose acetate phthalate polymer. Saudi Pharm J. 2017;25:921–6. https://doi.org/10.1016/j.jsps.2017.02.004.
21. Li M, Gao M, Fu Y, Chen C, Meng X, Fan A, *et al.* Acetal-linked polymeric prodrug micelles for enhanced curcumin delivery. Colloids Surf B. 2016;140:11–8. https://doi.org/10.1016/j.colsurfb.2015.12.025.
22. Li H, Li M, Chen C, Fan A, Kong D, Wang Z, *et al.* On-demand combinational delivery of curcumin and doxorubicin via a pH-labile micellar nanocarrier. Int J Pharm. 2015;495(1):572–8. https://doi.org/10.1016/j.ijpharm.2015.09.022.
23. Cao Y, Gao M, Chen C, Fan A, Zhang J, Kong D, *et al.* Triggered-release polymeric conjugate micelles for on-demand intracellular drug delivery. Nanotechnology. 2015;26:115101. https://doi.org/10.1088/0957-4484/26/11/115101.
24. Wang Z, Chen C, Zhang Q, Gao M, Zhang J, Kong D, *et al.* Tuning the architecture of polymeric conjugate to mediate intracellular delivery of pleiotropic curcumin. Eur J Pharm Biopharm. 2015;90:53–62. https://doi.org/10.1016/j.ejpb.2014.11.002.
25. Pathan IB, Jaware BP, Shelke S, Ambekar W. Curcumin loaded ethosomes for transdermal application: formulation, optimization, in-vitro and in-vivo study. J Drug Deliv Sci Technol. 2018;44:49–57. https://doi.org/10.1016/j.jddst.2017.11.005.

26. Gupta NK, Dixit VK. Development and evaluation of vesicular system for curcumin delivery. Arch Dermatol Res. 2011;303:89–101. https://doi.org/10.1007/s00403-010-1096-6.
27. Naik A, Kalia YN, Guy RH, Fessi H. Enhancement of topical delivery from biodegradable nanoparticles. Pharm Res. 2004;21:1818–25.
28. Abdel-Hafez SM, Hathout RM, Sammour OA. Tracking the transdermal penetration pathways of optimized curcumin-loaded chitosan nanoparticles via confocal laser scanning microscopy. Int J Biol Macromol. 2018;108:753–64. https://doi.org/10.1016/j.ijbiomac.2017.10.170.
29. Merisko-Liversidge EM, Liversidge GG. Drug nanoparticles: formulating poorly water-soluble compounds. Toxicol Pathol. 2008;36:43–8. https://doi.org/10.1177/0192623307310946.
30. Kean T, Thanou M. Biodegradation, biodistribution and toxicity of chitosan. Adv Drug Deliv Rev. 2010;62:3–11. https://doi.org/10.1016/j.addr.2009.09.004.
31. Wedmore I, McManus JG, Pusateri AE, Holcomb JB. A special report on the chitosan-based hemostatic dressing: experience in current combat operations. J Trauma. 2006;60:655–8. https://doi.org/10.1097/01.ta.0000199392.91772.44.
32. Gan Q, Wang T, Cochrane C, McCarron P. Modulation of surface charge, particle size and morphological properties of chitosan–TPP nanoparticles intended for gene delivery. Colloids Surf B. 2005;44:65–73.
33. Koukaras EN, Papadimitriou SA, Bikiaris DN, Froudakis GE. Insight on the formation of chitosan nanoparticles through ionotropic gelation with tripolyphosphate. Mol Pharm. 2012;9:2856–62.
34. Taveira SF, Nomizo A, Lopez RFV. Effect of the iontophoresis of a chitosan gel on doxorubicin skin penetration and cytotoxicity. J Control Release. 2009;134:35–40. https://doi.org/10.1016/j.jconrel.2008.11.002.
35. Calvo P, Remunan-Lopez C, Vila-Jato J, Alonso M. Novel hydrophilic chitosan-polyethylene oxide nanoparticles as protein carriers. J Appl Polym Sci. 1997;63:125–32.
36. Chuah LH, Billa N, Roberts CJ, Burley JC, Manickam S. Curcumin-containing chitosan nanoparticles as a potential mucoadhesive delivery system to the colon. Pharm Dev Technol. 2013;18:591–9. https://doi.org/10.3109/10837450.2011.640688.
37. Luo Y, Zhang B, Cheng W-H, Wang Q. Preparation, characterization and evaluation of selenite-loaded chitosan/TPP nanoparticles with or without zein coating. Carbohydr Polym. 2010;82:942–51.
38. Amekyeh H, Billa N, Yuen K-H, Chin SLS. A gastrointestinal transit study on amphotericin b-loaded solid lipid nanoparticles in rats. AAPS PharmSciTech. 2015;16:871–7.
39. Pawar HA, Mane SS, Attarde VB. Novel vesicular drug delivery system for topical delivery of indomethacin. Drug Deliv Lett. 2015;5:40–51.
40. Ajun W, Yan S, Li G, Huili L. Preparation of aspirin and probucol in combination loaded chitosan nanoparticles and in vitro release study. Carbohydr Polym. 2009;75:566–74. https://doi.org/10.1016/j.carbpol.2008.08.019.
41. Nair RS, Nair S. Permeation studies of captopril transdermal films through human cadaver skin. Curr Drug Deliv. 2015;12:517–23.
42. Chen H, Chang X, Du D, Li J, Xu H, Yang X. Microemulsion-based hydrogel formulation of ibuprofen for topical delivery. Int J Pharm. 2006;315:52–8.
43. Rajesh S, Sujith S. Permeation of flurbiprofen polymeric films through human cadaver skin. Int J Pharm Tech Res. 2013;5:177–82.
44. Ohya Y, Shiratani M, Kobayashi H, Ouchi T. Release behavior of 5-fluorouracil from chitosan-gel nanospheres immobilizing 5-fluorouracil coated with polysaccharides and their cell specific cytotoxicity. J Macromol Sci A. 1994;31:629–42.
45. Fan W, Yan W, Xu Z, Ni H. Formation mechanism of monodisperse, low molecular weight chitosan nanoparticles by ionic gelation technique. Colloids Surf B. 2012;90:21–7.
46. Shu X, Zhu K. The influence of multivalent phosphate structure on the properties of ionically cross-linked chitosan films for controlled drug release. Eur J Pharm Biopharm. 2002;54:235–43.
47. Wang QZ, Chen XG, Liu N, Wang SX, Liu CS, Meng XH, *et al*. Protonation constants of chitosan with different molecular weight and degree of deacetylation. Carbohydr Polym. 2006;65:194–201. https://doi.org/10.1016/j.carbpol.2006.01.001.
48. Kotze AF, Thanou MM, Luessen HL, de Boer BG, Verhoef JC, Junginger HE. Effect of the degree of quaternization of N-trimethyl chitosan chloride on the permeability of intestinal epithelial cells (Caco-2). Eur J Pharm Biopharm. 1999;47:269–74.
49. Hamman JH, Stander M, Kotzé AF. Effect of the degree of quaternisation of N-trimethyl chitosan chloride on absorption enhancement: in vivo evaluation in rat nasal epithelia. Int J Pharm. 2002;232:235–42. https://doi.org/10.1016/S0378-5173(01)00914-0.
50. He W, Guo X, Xiao L, Feng M. Study on the mechanisms of chitosan and its derivatives used as transdermal penetration enhancers. Int J Pharm. 2009;382:234–43. https://doi.org/10.1016/j.ijpharm.2009.07.038.
51. Gallo RL, Hooper LV. Epithelial antimicrobial defence of the skin and intestine. Nat Rev Immunol. 2012;12:503–16. https://doi.org/10.1038/nri322853.
52. de Pinho Neves AL, Milioli CC, Müller L, Riella HG, Kuhnen NC, Stulzer HK. Factorial design as tool in chitosan nanoparticles development by ionic gelation technique. Colloid Surf A. 2014;445:34–9.
53. Grenha A, Seijo B, Serra C, Remuñán-López C. Chitosan nanoparticle-loaded mannitol microspheres: structure and surface characterization. Biomacromolecules. 2007;8:2072–9. https://doi.org/10.1021/bm061131g.
54. Wan S, Sun Y, Qi X, Tan F. Improved bioavailability of poorly water-soluble drug curcumin in cellulose acetate solid dispersion. AAPS PharmSciTech. 2012;13:159–66. https://doi.org/10.1208/s12249-011-9732-9.
55. Chereddy KK, Coco R, Memvanga PB, Ucakar B, des Rieux A, Vandermeulen G, *et al*. Combined effect of PLGA and curcumin on wound healing activity. J Control Release. 2013;171:208–15. https://doi.org/10.1016/j.jconrel.2013.07.015.
56. Naghibzadeh M, Amani A, Amini M, Esmaeilzadeh E, Mottaghi-Dastjerdi N, Faramarzi MA. An insight into the interactions between α-tocopherol and chitosan in ultrasound-prepared nanoparticles. J Nanomater. 2010;2010:44.
57. Singh AV, Nath LK. Synthesis and evaluation of physicochemical properties of cross-linked sago starch. Int J Biol Macromol. 2012;50:14–8.
58. Paradkar A, Ambike AA, Jadhav BK, Mahadik KR. Characterization of curcumin–PVP solid dispersion obtained by spray drying. Int J Pharm. 2004;271:281–6. https://doi.org/10.1016/j.ijpharm.2003.11.014.
59. Sarmento B, Ferreira D, Veiga F, Ribeiro A. Characterization of insulin-loaded alginate nanoparticles produced by ionotropic pre-gelation through DSC and FTIR studies. Carbohydr Polym. 2006;66:1–7. https://doi.org/10.1016/j.carbpol.2006.02.008.61.
60. Borges O, Borchard G, Verhoef JC, de Sousa A, Junginger HE. Preparation of coated nanoparticles for a new mucosal vaccine delivery system. Int J Pharm. 2005;299:155–66. https://doi.org/10.1016/j.ijpharm.2005.04.037.
61. Parize AL, Stulzer HK, Laranjeira MCM, da Costa Brighente IM, de Souza TCR. Evaluation of chitosan microparticles containing curcumin and crosslinked with sodium tripolyphosphate produced by spray drying. Quim Nova. 2012;35:1127–32.
62. Dudhani AR, Kosaraju SL. Bioadhesive chitosan nanoparticles: preparation and characterization. Carbohydr Polym. 2010;81:243–51.
63. Tsai M-L, Chen R-H, Bai S-W, Chen W-Y. The storage stability of chitosan/tripolyphosphate nanoparticles in a phosphate buffer. Carbohydr Polym. 2011;84:756–61. https://doi.org/10.1016/j.carbpol.2010.04.040.
64. Hariharan S, Bhardwaj V, Bala I, Sitterberg J, Bakowsky U, Ravi Kumar MNV. Design of estradiol loaded PLGA Nanoparticulate formulations: a potential oral delivery system for hormone therapy. Pharm Res. 2006;23:184–95. https://doi.org/10.1007/s11095-005-8418-y.

65. Ko J, Park HJ, Hwang S, Park J, Lee J. Preparation and characterization of chitosan microparticles intended for controlled drug delivery. Int J Pharm. 2002;249:165–74.67.
66. Katas H, Hussain Z, Ling TC. Chitosan nanoparticles as a percutaneous drug delivery system for hydrocortisone. J Nanomater. 2012;2012:45.
67. Uchida T, Kadhum WR, Kanai S, Todo H, Oshizaka T, Sugibayashi K. Prediction of skin permeation by chemical compounds using the artificial membrane, Strat-M™. Eur J Pharm Sci. 2015;67:113–8. https://doi.org/10.1016/j.ejps.2014.11.002.
68. Tiyaboonchai W, Tungpradit W, Plianbangchang P. Formulation and characterization of curcuminoids loaded solid lipid nanoparticles. Int J Pharm. 2007;337:299–306. https://doi.org/10.1016/j.ijpharm.2006.12.043.
69. Sartorelli P, Andersen HR, Angerer J, Corish J, Drexler H, Göen T, *et al*. Percutaneous penetration studies for risk assessment. Environ Toxicol Pharmacol. 2000;8:133–52. https://doi.org/10.1016/S1382-6689(00)00035-1.71.
70. Ruela ALM, Perissinato AG, Lino MES, Mudrik PS, Pereira GR. Evaluation of skin absorption of drugs from topical and transdermal formulations. Braz J Pharm Sci. 2016;52:527–44.
71. Ratanajiajaroen P, Watthanaphanit A, Tamura H, Tokura S, Rujiravanit R. Release characteristic and stability of curcumin incorporated in β-chitin non-woven fibrous sheet using Tween 20 as an emulsifier. Eur Polym J. 2012;48:512–23. https://doi.org/10.1016/j.eurpolymj.2011.11.020.
72. Doaa Nabih M, Sanjay RM, Lijia W, Abd-Elgawad Helmy A-E, Osama Abd-Elazeem S, Marwa Salah E-D, *et al*. Water-soluble complex of curcumin with cyclodextrins: enhanced physical properties for ocular drug delivery. Curr Drug Deliv. 2017;14:875–86. https://doi.org/10.2174/1567201813666160808111209.74.
73. Hasanovic A, Zehl M, Reznicek G, Valenta C. Chitosan-tripolyphosphate nanoparticles as a possible skin drug delivery system for aciclovir with enhanced stability. J Pharm Pharmacol. 2009;61(12):1609–16.
74. Sun J, Han J, Zhao Y, Zhu Q, Hu J. Curcumin induces apoptosis in tumor necrosis factor-alpha-treated HaCaT cells. Int J Immunopharmacol. 2012;13:170–4. https://doi.org/10.1016/j.intimp.2012.03.025.
75. Scharstuhl A, Mutsaers H, Pennings S, Szarek W, Russel F, Wagener F. Curcumin-induced fibroblast apoptosis and in vitro wound contraction are regulated by antioxidants and heme oxygenase: implications for scar formation. J Cell Mol Med. 2009;13:712–25.